

香菇生物质基氮掺杂微孔碳材料的制备及其在超级电容器中的应用

胡青桃¹ 张文达¹ 李涛¹ 晏晓东^{*1} 顾志国^{*1,2}

(¹江南大学化学与材料工程学院, 无锡 214122)

(²合成与生物胶体教育部重点实验室, 无锡 214122)

摘要: 采用简易浸泡法和一步碳化/活化法制备香菇生物质基氮掺杂微孔碳材料(NMCs), 利用扫描电子显微镜(SEM)、透射电子显微镜(SEM)、X射线衍射(XRD)和X射线光电子能谱(XPS)对材料的结构形貌进行表征, 并研究了其超级电容特性。测试结果表明, NMCs的微孔比表面积高达 $1\ 594\ \text{m}^2\cdot\text{g}^{-1}$, 且拥有更高数量的含氮官能团, 其吡啶型含氮官能团比例也有所提高, 展现出优异的超级电容特性。在 $0.5\ \text{A}\cdot\text{g}^{-1}$ 的电流密度下, 其比容量高达 $325\ \text{F}\cdot\text{g}^{-1}$, 当电流密度上升到 $20\ \text{A}\cdot\text{g}^{-1}$ 时, 其比电容仍然高达 $180\ \text{F}\cdot\text{g}^{-1}$, 表现出优异的倍率性能; 同时, 在 $5\ \text{A}\cdot\text{g}^{-1}$ 的电流密度下, 电极经历5 000次充放电循环后具有97.7%的比容量保持率, 展现出优异的循环稳定性。这主要归因于NMCs超高的微孔比表面积和丰富的含氮官能团。

关键词: 超级电容器; 碳; 微孔材料; 炭化; 氮掺杂

中图分类号: O646.54 文献标识码: A 文章编号: 1001-4861(2020)08-1573-09

DOI: 10.11862/CJIC.2020.114

Preparation and Application in Supercapacitors of Shiitake Biomass-Based Nitrogen-Doped Microporous Carbon

HU Qing-Tao¹ ZHANG Wen-Da¹ LI Tao¹ YAN Xiao-Dong^{*1} GU Zhi-Guo^{*1,2}

(¹School of Chemistry and Material Engineering, Jiangnan University, Wuxi, Jiangsu 214122, China)

(²Key Laboratory of Synthetic and Biological Colloids, Ministry of Education, Wuxi, Jiangsu 214122, China)

Abstract: Shiitake-derived nitrogen-doped microporous carbon materials were prepared by a simple activation/carbonization process. It was found that the nitrogen content was enhanced owing to the consumption of carbon in the activation process, and that the pyridinic nitrogen groups were promoted after activation. The microporous carbons offered a high specific surface area of $1\ 930\ \text{m}^2\cdot\text{g}^{-1}$ with a high micropore surface area of $1\ 594\ \text{m}^2\cdot\text{g}^{-1}$. The high micropore surface area accompanied with rich nitrogen and oxygen groups contributed to a remarkable specific capacitance of $325\ \text{F}\cdot\text{g}^{-1}$ at $0.5\ \text{A}\cdot\text{g}^{-1}$ and high rate capability. In addition, shiitake-derived microporous carbons presented robust cycling stability with 2.3% capacitance loss during 5 000 cycles, and a high specific capacitance of $203\ \text{F}\cdot\text{g}^{-1}$ at $0.5\ \text{A}\cdot\text{g}^{-1}$ in symmetric supercapacitors. The high performance could be attributed to the high surface area, enhancing electric double layer capacitance, and numerous nitrogen groups.

Keywords: supercapacitors; carbon; microporous materials; carbonization; nitrogen doping

Carbon-based supercapacitors are well-known for their long cycle life, relatively high energy density and high power density^[1-2]. These merits originate from the unique energy storage/conversion process of electric

收稿日期: 2020-01-13. 收修改稿日期: 2020-03-13.

国家自然科学基金(No.21905116, 21771089)、中央高校基础研究经费(No.JUSRP11930, JUSRP51725B, JUSRP21936)和江苏省自然科学基金(No.BK20190614)资助。

*通信联系人。E-mail: ; 会员登记号: xiaodong.yan@jiangnan.edu.cn, zhiguogu@jiangnan.edu.cn

double layer capacitors. Electrostatic charge accumulation at the carbon electrode/electrolyte interface forms the electric double layer that enables the energy storage and release rapidly^[2]. Therefore, the capacitance of carbon-based supercapacitors is proportional to the specific surface area of the carbon electrode materials^[2-3], and activated carbons dominate the electrode materials for supercapacitors due to their high surface area, good conductivity, low cost, and easy processability.

Since the first usage of porous carbon in supercapacitors by Becker in 1957^[4], various activated carbon materials have been studied as electrode materials for supercapacitors^[5-13], aiming to find high-capacitance porous carbons. With more research efforts and interests devoted to the study of porous carbon electrode materials, researchers found that the capacitance of porous carbons is not only dependent on their specific surface area, but also related to pore size and pore shape^[14-15]. Particularly, micropores are considered to play a decisive role in enhancing the capacitance^[14-15]. Though activation method is a mature manufacturing technique that is widely used worldwide and is still preferred to produce low-cost porous carbons for supercapacitors, it is very difficult to produce microporous carbons. By reviewing the literature, it is concluded that the physicochemical properties of the precursors can greatly affect the porous structures of the resulted activated carbons. For example, fibrous precursors will more likely evolve into microporous carbons^[15-17], and many biomass materials can be easily transformed into microporous carbons by common activation methods.^[18]

On the other hand, biomass materials are sustainable precursors which are critical to the long-term development of carbon-based supercapacitors. In addition, biomass-derived carbons usually contain various heteroatoms such as nitrogen and oxygen, which contribute to high pseudocapacitance owing to the reversible redox reactions of the heteroatom groups, raising the capacitance of carbon materials up to 300~350 F·g⁻¹ in aqueous electrolytes^[19-24]. KOH is a commonly used activator, but a high KOH/biomass

mass ratio of 3~4 is usually needed to carbonize/activate the biomass materials^[19,21,23]. The presence of abundant KOH leads to strong corrosion of the instruments/equipment, high cost, low carbon yield, *etc.* Herein, we took full advantage of the intrinsic porous structure of dry shiitake mushrooms to achieve high-surface-area nitrogen-doped microporous nanocarbons at a low KOH/biomass mass ratio of 0.3 by a simple one-step carbonization/activation process. The high-surface-area microporous carbons with rich nitrogen groups demonstrated high specific capacitance, excellent cycling stability, and remarkable rate capability.

1 Experimental

1.1 Preparation of microporous carbons

In a typical synthesis, two pieces of dry shiitake mushrooms were soaked in 1.0 mol·L⁻¹ KOH aqueous solution for 10 h. Then the shiitake mushrooms were transferred from the alkaline solution to a petri dish and dried at 100 °C overnight in an oven. The weight ratio of dry shiitake to KOH was about 0.3. The carbonization/activation process was carried out at 800 °C for 3 h under nitrogen atmosphere with a heating rate of 5 °C·min⁻¹. The product was washed with abundant 0.1 mol·L⁻¹ HCl aqueous solutions, plenty of deionized water until neutral pH, and dried at 120 °C for 5 h. The as-prepared product was the microporous carbons (NMCs). For comparison, dry shiitake mushrooms were directly carbonized at 800 °C for 3 h under nitrogen atmosphere with a heating rate of 5 °C·min⁻¹, and the product was designated as NCs.

1.2 Materials characterization

Scanning electron microscopy (SEM) and transmission electron microscopy (TEM) were used to examine the morphologies of the samples. The SEM images were collected on a Hitachi S4700 scanning electron microscope at 3.0 kV, and the TEM images were obtained on a JEOL JEM-3010 transmission electron microscope at 200 kV. The powder X-ray diffraction (XRD) patterns were collected on a Bruker D8 Venture diffractometer from 10° to 90° using a Cu K α radiation source (40 kV, 40 mA, λ =0.154 nm). X-

ray photoelectron spectroscopy (XPS) measurements were carried out with an AXIS Supra by Kratos Analytical Inc. using monochromatic Al X-ray ($h\nu = 1486.6$ eV) as the excitation source. All XPS spectra were calibrated by C1s signal at 284.8 eV. N_2 adsorption-desorption isotherm was measured at 77 K with a Quantachrome QUADRASORB SI instrument after the samples were degassed at 573 K for 4 h. Brunauer-Emmett-Teller (BET) model was performed to measure the specific surface area. Micropore surface area was calculated by $V-t$ method. Pore volume, average pore size and pore size distribution were analyzed based on density functional theory (DFT) method.

1.3 Electrochemical characterization

To prepare the working electrodes, the samples and the polyvinylidene fluoride binder with the mass ratio of 9 were dispersed in 1-methyl-2-pyrrolidone. The as-prepared slurry was coated on the Pt plates. The electrodes were dried at 120 °C for 10 h in a vacuum oven. The mass of active materials on each Pt plate was about $3.0 \text{ mg}\cdot\text{cm}^{-2}$. The electrochemical measurements were separately carried out in a three-electrode system and in a two-electrode system. $1 \text{ mol}\cdot\text{L}^{-1} \text{ H}_2\text{SO}_4$ aqueous solution was used as the electrolyte. Cyclic voltammetry (CV) and electrochemical impedance spectroscopy (EIS) measurements in the frequency range of $10^3 \text{ kHz}\sim 10 \text{ mHz}$ at an open circuit potential with an amplitude of 5 mV were performed on a CHI760E electrochemical workstation. The galvanostatic charge/discharge profiles were obtained on a LAND CT2001A system.

In the three-electrode system, an Ag/AgCl electrode ($3.5 \text{ mol}\cdot\text{L}^{-1} \text{ KCl}$, 0.2046 V vs standard hydrogen electrode at 25 °C) and a platinum plate were used as the reference electrode and the counter electrode, respectively. The capacitance was calculated according to the following equation^[25]:

$$C_s = I\Delta t / (m\Delta V)$$

where C_s is the specific capacitance ($\text{F}\cdot\text{g}^{-1}$), I is the current density ($\text{A}\cdot\text{g}^{-1}$), Δt is the discharge time (s), ΔV is the potential window (V), and m is the mass of the active materials on each electrode.

In the two-electrode system, CV and galvanostatic

charge/discharge measurements were carried out in the potential range of 0~1.0 V. The specific capacitance was calculated based on the following equation^[25-26]:

$$C = 2I\Delta t / (m\Delta V)$$

where C is the specific capacitance ($\text{F}\cdot\text{g}^{-1}$). The specific energy density E ($\text{Wh}\cdot\text{kg}^{-1}$) and the power density P ($\text{W}\cdot\text{kg}^{-1}$) were obtained by the following two equations^[25]:

$$E = (1/4) \times (1/3.6) \times C(\Delta V)^2$$

$$P = 3600E/\Delta t$$

2 Results and discussion

Fig. 1A showed the digital image of dry shiitake mushrooms. Shiitake was selected as the carbon source because shiitake mushrooms were full of air-filled cavities with a size of several micrometers (Fig. 1B) and presented high water absorbing capacity (weight ratio of water to dry shiitake was ~5). Plenty of KOH aqueous solution could be locked in the cavities of shiitake mushrooms. Once the water was evaporated, KOH was uniformly coated on the walls of each cavity which favors a thorough activation of shiitake mushrooms for high specific surface area. The KOH/shiitake mass ratio was about 0.3. Fig. 1C displayed the SEM image of NCs. The morphology was similar to that of the dry shiitake (Fig. 1A). Magnified SEM image showed the relatively smooth surface of NCs (Fig. 1D). The activation process disintegrated the structure of dry shiitake owing to the drastic activation reaction, and the NMCs showed granular morphology (Fig. 1E). Magnified SEM image showed that the size of NMCs at least in one dimension was within 200 nm (Fig. 1F). This confirmed the advantage of shiitake to produce nanosized porous carbons. TEM image demonstrated many macropores in NCs (Fig. 1G), and the high-resolution TEM (HRTEM) image indicated the amorphous nature of NCs (Fig. 1H). As depicted by Fig. 1I, NMCs present a sheet-like structure with a thin thickness, confirming the nanosized structure. HRTEM demonstrated the microporous structure of NMCs with pore sizes within ~2 nm (Fig. 1J). XRD analysis were further carried out to study the microstructures of NCs and NMCs. Fig. 2 presented the XRD profiles of NCs

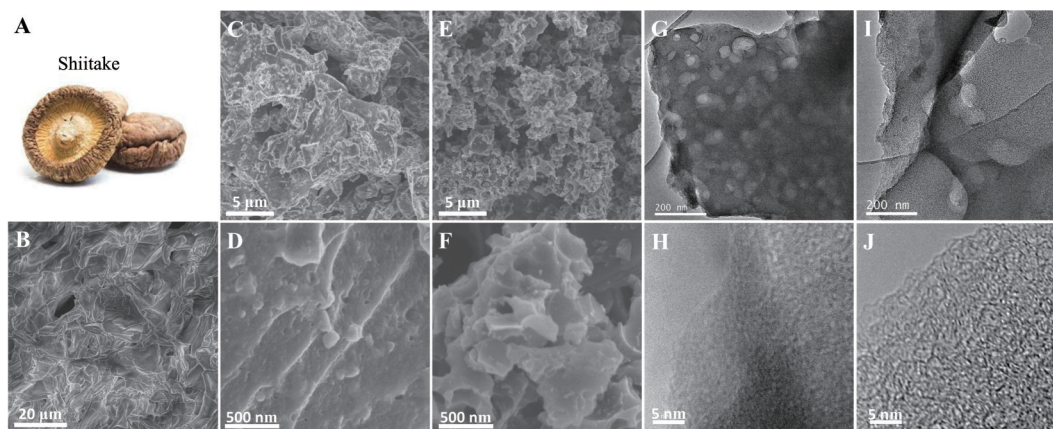


Fig.1 (A) Digital and (B) SEM images of dry shiitake mushrooms; SEM images of (C, D) NCs and (E, F) NMCs; TEM images of (G, H) NCs and (I, J) NMCs

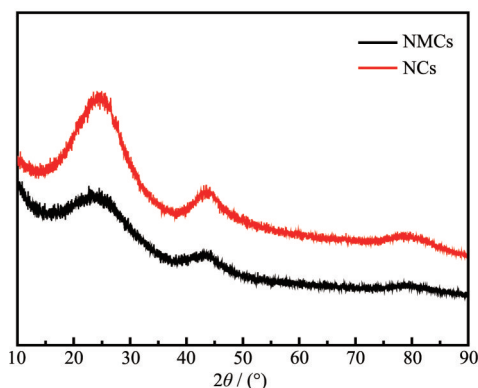


Fig.2 XRD patterns of NCs and NMCs

and NMCs. NMCs had a more disordered structure than NCs as indexed by the less intensified diffraction peaks at around 25° and 43.5° due to the activation reaction.

Nitrogen adsorption-desorption measurement was employed to evaluate the porous structures of NCs and NMCs. All the data were summarized in Table 1. The isotherm of NMCs showed a type- I curve with a sharp nitrogen adsorption at relative pressures below 0.1 (Fig. 3A). This indicated that NMCs possessed microporous structure and high porosity (pore volume: $0.863 \text{ cm}^3 \cdot \text{g}^{-1}$)^[27]. The BET surface area of NMCs was as large as $1\,930 \text{ m}^2 \cdot \text{g}^{-1}$ with a high micropore surface area of $1\,594 \text{ m}^2 \cdot \text{g}^{-1}$. In contrast, NCs showed limited nitrogen uptake, suggesting low porosity (pore volume: 0.073

$\text{cm}^3 \cdot \text{g}^{-1}$). The BET surface area of NCs was calculated to be only $63 \text{ m}^2 \cdot \text{g}^{-1}$. Fig. 3B showed the pore size distribution of NCs and NMCs calculated by DFT method. The pore size of NMCs was in the range from 0.5 to 3 nm, concentrating at 0.7 and 1.2 nm. The average pore size of NMCs was ~ 2.05 nm, which was consistent with the HRTEM observation. NCs presented a large average pore size of 5.27 nm with negligible micropores (Fig. 3B). It was thus highly efficient to synthesize high-surface-area microporous nanocarbons with shiitake by KOH activation.

XPS measurement was performed to reveal the elemental composition and chemical structure of NMCs and NCs. Fig. 3C showed the XPS survey spectra of NCs and NMCs. It was found that shiitake - based carbons contained abundant nitrogen and oxygen heteroatoms. This was good for enhancing the specific capacitance by pseudo-capacitance from redox reactions of heteroatom groups^[28-30]. The N contents of NCs and NMCs were 1.4% and 2.1%(n/n), respectively, while the O contents of NCs and NMCs were 11.4% and 14.1%(n/n), respectively. NMCs displayed a higher N content than NCs because of the consumption of some carbon in the activation reaction. Nitrogen groups were believed to improve the surface wettability of carbons and further favored the surface kinetics during

Table 1 Summary of key parameter from N_2 adsorption-desorption analyses

Material	BET surface area / ($\text{m}^2 \cdot \text{g}^{-1}$)	Micropore surface area / ($\text{m}^2 \cdot \text{g}^{-1}$)	Pore volume / ($\text{cm}^3 \cdot \text{g}^{-1}$)	Average pore size / nm
NMCs	1 930	1 594	0.863	2.05
NCs	63	0	0.073	5.27

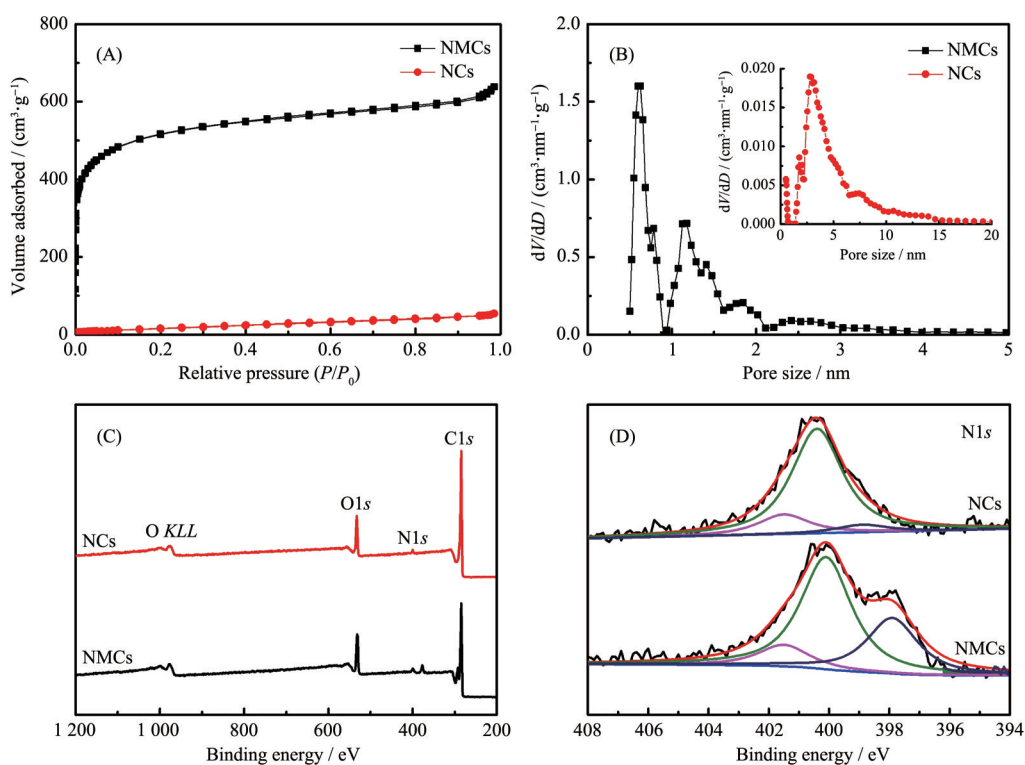


Fig.3 (A) Nitrogen adsorption/desorption isotherms, (B) pore size distribution, (C) XPS survey spectra, and (D) N1s XPS spectra of NCs and NMCs

the energy storage process^[31]. The N1s spectrum (Fig. 3D) was fitted into three parts: the signals at around 398, 400, and 401 eV were attributed to pyridinic nitrogen (N-6), pyrrolic nitrogen (N-5), and quaternary nitrogen (N-Q), respectively^[28-29,32]. NMCs had a much higher content of N-6 than NCs as evidenced by the fitted N1s spectra, which greatly enhanced the pseudocapacitance^[33]. In addition, N-Q groups could improve the conductivity of carbons^[34].

Electrochemical properties of NMCs and NCs were firstly investigated in the potential window of $-0.1\sim 0.9$ V vs Ag/AgCl in a three-electrode system. Fig. 4A showed the CV curves of NCs and NMCs at $5\text{ mV}\cdot\text{s}^{-1}$. Both NCs and NMCs presented rectangular-shaped CV curves, indicative of the domination of electric double layer capacitive behavior. The CV curve of NMCs displayed much larger redox reaction peaks, indicating enhanced pseudo-capacitance. This was consistent with the XPS analysis that NMCs had a relatively higher nitrogen content. Fig. 4B demonstrated the galvanostatic charge-discharge profiles of NCs and NMCs at $0.5\text{ A}\cdot\text{g}^{-1}$. The galvanostatic charge or

discharge profile significantly deviated from linear shape due to the faradaic reactions of heteroatom groups. The charge-discharge time of the NMCs electrode approached 3 times that of the NCs electrode. Rate capability of NCs and NMCs was evaluated by varying current density. Specific capacitances at various current densities were displayed in Fig. 4C. The specific capacitance of NMCs at $0.5\text{ A}\cdot\text{g}^{-1}$ was $325\text{ F}\cdot\text{g}^{-1}$, while it was only $114\text{ F}\cdot\text{g}^{-1}$ for NCs. More importantly, the specific capacitance of NMCs still reached as high as $180\text{ F}\cdot\text{g}^{-1}$ at a high current density of $20\text{ A}\cdot\text{g}^{-1}$, which accounted for 55% of the value at $0.5\text{ A}\cdot\text{g}^{-1}$. For comparison, the specific capacitance of NCs at $20\text{ A}\cdot\text{g}^{-1}$ was only 44% of that at $0.5\text{ A}\cdot\text{g}^{-1}$. These results implied that NMCs possessed high energy storage capability and good rate capability. The shape of the CV curves of the NMCs electrode only slightly deviated with increasing scan rate (Fig. 4D), confirming the high rate capability of NMCs.

Kinetics at the electrode/electrolyte interface were further disclosed by EIS measurement. The Nyquist plots showed one semicircle in the high-frequency

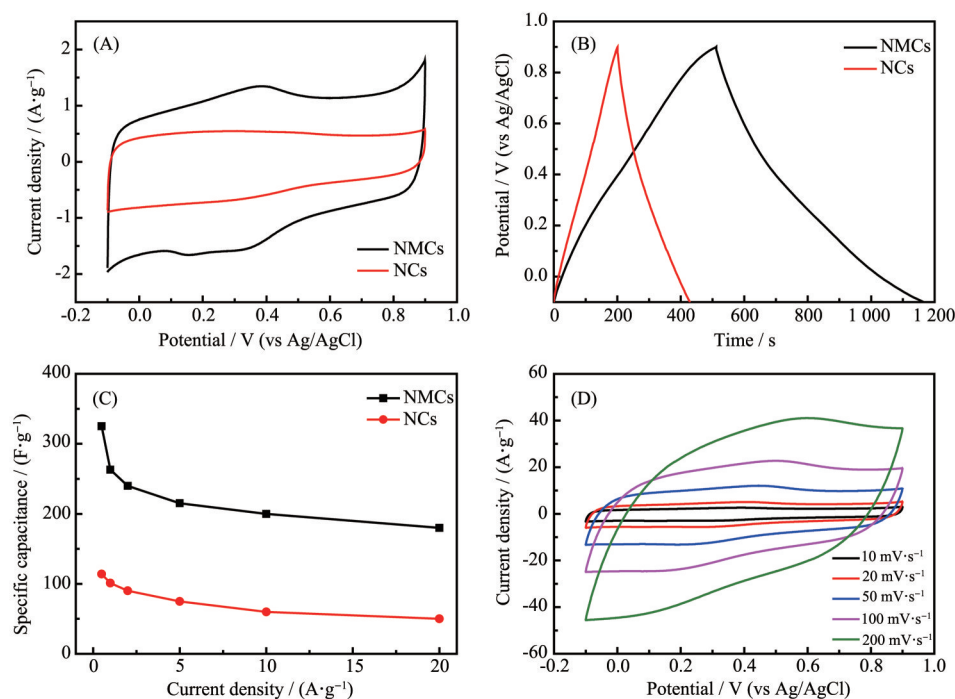


Fig.4 (A) CV curves at $5 \text{ mV} \cdot \text{s}^{-1}$, (B) charge/discharge profiles at $0.5 \text{ A} \cdot \text{g}^{-1}$, and (C) rate capability of NCs and NMCs; (D) CV curves of an NMCs electrode at various scan rates

region and a linear line in the low-frequency region (Fig. 5A). In general, the larger the slope of the linear part, the faster the electric double layer will be formed^[34]. Obviously, ion diffusion was much faster on the NMCs electrode. The diameter of the semicircle indexed the charge transfer resistance (R_{ct}). The R_{ct} values of the NMCs and NCs electrodes were $0.35 \text{ } \Omega$ and $0.45 \text{ } \Omega$, respectively, confirming faster charge transfer process on the surface of NMCs. The intercept of the Nyquist plot with x axis represented the equivalent series resistance (R_s) from the electrolyte, current collector, electrode/electrolyte interface, etc. The NMCs electrodes had smaller R_s ($1.15 \text{ } \Omega$) than the NCs

electrodes ($1.51 \text{ } \Omega$). Excitingly, NMCs exhibited outstanding cycling stability with a small capacitance loss of 2.3% during the first 200 cycles and with no capacitance loss during the following 4 800 cycles (Fig. 5B). The capacitance loss during the initial 200 cycles might be due to the presence of some unstable oxygen groups^[35].

To explore the practical applications of NMCs in supercapacitors, symmetric supercapacitors fabricated from NMCs were tested. Fig. 6A showed the CV curves of a NMCs supercapacitor. The CV curves displayed a rectangular shape, which was the typical shape of the CV curves of electric double layer capacitors. The CV

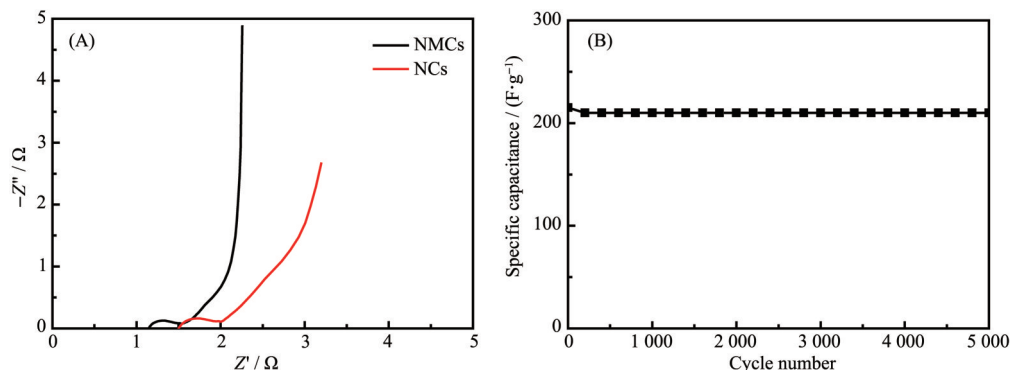


Fig.5 (A) EIS spectra of NCs and NMCs electrodes; (B) Stability test at a current density of $5 \text{ A} \cdot \text{g}^{-1}$ in a three-electrode system

curve maintained its rectangular shape as the scan rate increased up to $200 \text{ mV}\cdot\text{s}^{-1}$, confirming its excellent rate capability. The charge/discharge profiles at different current densities demonstrated near-triangular shape and small ohmic loss (Fig. 6B). These indicated good capacitive properties of NMCs in real supercapacitors.

The specific capacitance was plotted against the current density (Fig. 6C). The specific capacitance at $0.5 \text{ A}\cdot\text{g}^{-1}$ was $203 \text{ F}\cdot\text{g}^{-1}$, and still reached $120 \text{ F}\cdot\text{g}^{-1}$ at $20 \text{ A}\cdot\text{g}^{-1}$, outperforming many other carbon electrode materials reported in the literature (Table 2) [25-26,36-40].

The specific capacitance at $20 \text{ A}\cdot\text{g}^{-1}$ was $\sim 60\%$ of that at $0.5 \text{ A}\cdot\text{g}^{-1}$, consolidating its remarkable rate capability. The small R_{ct} and near-vertical linear part suggested fast surface charge transfer kinetics, as indicated by the EIS spectrum (Fig. 6D). It thus could be concluded that NMCs had high capacitive performance and that the high performance could be ascribed to the high surface area, improved surface kinetics because of abundant nitrogen groups, and good conductivity.

The Ragone plot (power density vs energy density) was presented in Fig. 7. The NMCs supercapacitor

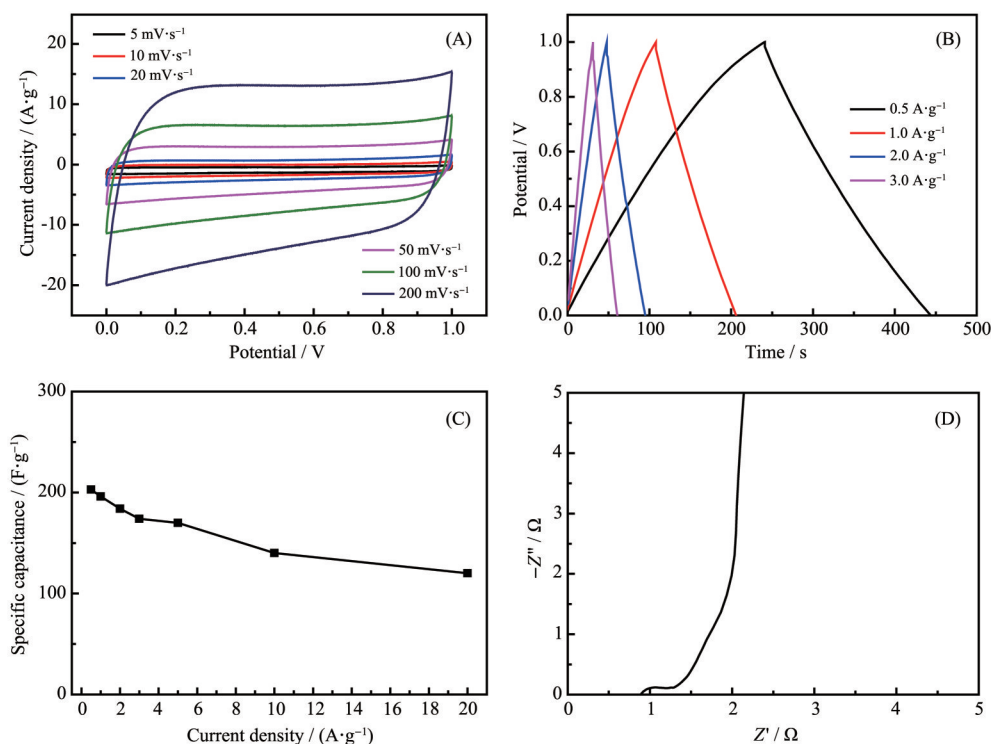


Fig.6 (A) CV curves at various scan rates, (B) charge/discharge profiles at different current densities, (C) rate capability, and (D) EIS spectrum of a symmetric NMCs supercapacitor

Table 2 Electrochemical performance of biomass-derived porous carbons in symmetric supercapacitors

Material	Electrolyte	BET surface area / ($\text{m}^2\cdot\text{g}^{-1}$)	C at $0.5 \text{ A}\cdot\text{g}^{-1}$	C at $10 \text{ A}\cdot\text{g}^{-1}$	Reference
Shiitake	$1 \text{ mol}\cdot\text{L}^{-1} \text{ H}_2\text{SO}_4$	1 930	203	140	This Work
Willow catkin	$1 \text{ mol}\cdot\text{L}^{-1} \text{ Na}_2\text{SO}_4$	1 533	170	100	[25]
Sisal	$6 \text{ mol}\cdot\text{L}^{-1} \text{ KOH}$	2 289	146	90	[26]
Broussonetia papyrifera	$6 \text{ mol}\cdot\text{L}^{-1} \text{ KOH}$	1 212	128	100	[36]
Loofah	$1 \text{ mol}\cdot\text{L}^{-1} \text{ Na}_2\text{SO}_4$	2 718	160	80	[37]
Pine cone	$1 \text{ mol}\cdot\text{L}^{-1} \text{ Na}_2\text{SO}_4$	1 515	135	<100	[38]
Cotton	PVA/KOH	399	170	<140	[39]
Black locust seed dregs	$6 \text{ mol}\cdot\text{L}^{-1} \text{ KOH}$	2 010	148	110	[40]

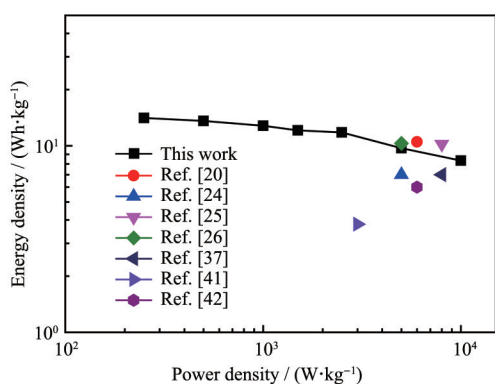


Fig.7 Energy density against powder density for different carbon materials

demonstrated a high energy density of $14.1 \text{ Wh}\cdot\text{kg}^{-1}$ at a power density of $180 \text{ W}\cdot\text{kg}^{-1}$. More importantly, it still achieved a high energy density of $11.1 \text{ Wh}\cdot\text{kg}^{-1}$ at a high power density of $\sim 5\ 700 \text{ W}\cdot\text{kg}^{-1}$. For comparison, the highest powder density values of the other carbon-based supercapacitors reported in the literature were plotted in the Ragone plot. Obviously, NMCs was one of the best electrode materials for high-rate supercapacitors^[20,24-26,37,41-42].

3 Conclusions

Shiitake-derived microporous nanocarbons with a high micropore surface area of $1\ 594 \text{ m}^2\cdot\text{g}^{-1}$ were synthesized by a simple one-step carbonization/activation process. The rich air-filled cavities in shiitake mushrooms made them ideal raw materials for high-surface-area porous nanocarbons with high accessible micropore surface area. The high micropore surface area and numerous nitrogen groups synergistically contributed to a high capacitance of $325 \text{ F}\cdot\text{g}^{-1}$ at $0.5 \text{ A}\cdot\text{g}^{-1}$, along with good rate capability ($180 \text{ F}\cdot\text{g}^{-1}$ at $20 \text{ A}\cdot\text{g}^{-1}$) and excellent cycling stability (2.3% capacitance loss in the period of 5 000 cycles). In symmetric supercapacitors, shiitake-derived microporous nanocarbons still presented a high capacitance of $203 \text{ F}\cdot\text{g}^{-1}$ at $0.5 \text{ A}\cdot\text{g}^{-1}$, making them promising electrode materials for high-performing supercapacitors.

References:

[1] Simon P, Gogotsi Y. *Nat. Mater.*, **2008**,**7**:845-854

- [2] Wang G P, Zhang L, Zhang J J. *Chem. Soc. Rev.*, **2012**,**41**:797-828
- [3] Zhang L L, Zhao X S. *Chem. Soc. Rev.*, **2009**,**38**:2520-2531
- [4] Ktz R, Carlen M. *Electrochim. Acta*, **2000**,**45**:2483-2498
- [5] ZHANG Ye-Qiong(张业琼), GONG Ye(丛野), ZHANG Jing(张静), et al. *Chinese J. Inorg. Chem.*(无机化学学报), **2018**, **34**(8):1430-1436
- [6] Balducci A, Dugas R, Taberna P L, et al. *J. Power Sources*, **2007**,**165**:922-927
- [7] Subramanian V, Luo C, Stephan A M, et al. *J. Phys. Chem. C*, **2007**,**111**:7527-7531
- [8] Hulicova - Jurcakova D, Seredych M, Lu G Q, et al. *Adv. Funct. Mater.*, **2009**,**19**:438-447
- [9] Wang G M, Wang H Y, Lu X H, et al. *Adv. Mater.*, **2014**,**26**:2676-2682
- [10] Li B, Dai F, Xiao Q F, et al. *Energy Environ. Sci.*, **2016**,**9**:102-106
- [11] Yu L Y, Hu L F, Anasori B, et al. *ACS Energy Lett.*, **2018**,**3**:1597-1603
- [12] MA Yan - Wen(马延文), XIONG Chuan - Yin(熊传银), HUANG Wen(黄雯), et al. *Chinese J. Inorg. Chem.*(无机化学学报), **2012**,**28**(3):546-550
- [13] To J W F, Chen Z, Yao H B, et al. *ACS Cent. Sci.*, **2015**,**1**:68-76
- [14] Chmiola J, Yushin G, Dash R, et al. *J. Power Sources*, **2006**, **158**:765-772
- [15] Jin Z, Yan X D, Yu Y H, et al. *J. Mater. Chem. A*, **2014**,**2**:11706-11715
- [16] Zhu K, Wang Y, Tang J A, et al. *Mater. Chem. Front.*, **2017**, **1**:958-966
- [17] Ma C, Song Y, Shi J L, et al. *Carbon*, **2013**,**51**:290-300
- [18] Abioye A M, Ani F N. *Renewable Sustainable Energy Rev.*, **2015**,**52**:1282-1293
- [19] Elmouwahidi A, Zapata - Benabithé Z, Carrasco - Marín F, et al. *Bioresour. Technol.*, **2012**,**111**:185-190
- [20] WU Zhong-Yu(武中钰), FAN Lei(范蕾), TAO You-Rong(陶友荣), et al. *Chinese J. Inorg. Chem.*(无机化学学报), **2018**, **34**(7):1249-1260
- [21] Peng C, Yan X B, Wang R T, et al. *Electrochim. Acta*, **2013**, **87**:401-408
- [22] Zhang J T, Gong L Y, Sun K, et al. *J. Solid State Electrochem.*, **2012**,**16**:2179-2186
- [23] Cheng P, Gao S Y, Zang P Y, et al. *Carbon*, **2015**,**93**:315-324
- [24] Chen Z Y, Sun J F, Bao R Q, et al. *ACS Sustainable Chem. Eng.*, **2019**,**7**:779-789
- [25] Li Y J, Wang G L, Wei T, et al. *Nano Energy*, **2016**,**19**:165-175
- [26] Li M L, Xiao H Y, Zhang T, et al. *ACS Sustainable Chem.*

- Eng.*, **2019**,**7**:4716-4723
- [27]Kunowsky M, Garcia-Gomez A, Barranco V, et al. *Carbon*, **2014**,**68**:553-562
- [28]Yan X D, Liu Y, Fan X R, et al. *J. Power Sources*, **2014**,**248**:745-751
- [29]Tan Y M, Xu C F, Chen G X, et al. *ACS Appl. Mater. Interfaces*, **2013**,**5**:2241-2248
- [30]Milczarek G, Ciszewski A, Stepniak I, et al. *J. Power Sources*, **2011**,**196**:7882-7885
- [31]Lota G, Grzyb B, Machnikowska H, et al. *Chem. Phys. Lett.*, **2005**,**404**:53-58
- [32]Chen L F, Zhang X D, Liang H W, et al. *ACS Nano*, **2012**,**6**:7092-7102
- [33]Li W R, Chen D H, Li Z, et al. *Electrochem. Commun.*, **2007**,**9**:569-573
- [34]Hassan F M, Chabot V, Li J D, et al. *J. Mater. Chem. A*, **2013**,**1**:2904-2912
- [35]Zhai Y P, Dou Y Q, Zhao D Y, et al. *Adv. Mater.*, **2011**,**23**(42):4828-4850
- [36]Wei T Y, Wei X L, Gao Y, et al. *Electrochim. Acta*, **2015**,**169**:186-194
- [37]Su X L, Chen J R, Zheng G P, et al. *Appl. Surf. Sci.*, **2018**,**436**:327-336
- [38]Bello A, Manyala N, Barzegar F, et al. *RSC Adv.*, **2016**,**6**:1800-1809
- [39]Fan Y M, Song W L, Li X G, et al. *Carbon*, **2017**,**111**:658-666
- [40]Hou L J, Hu Z A, Wang X T, et al. *J. Colloid Interface Sci.*, **2019**,**540**:88-96
- [41]Jia H Y, Sun J W, Xie X, et al. *Carbon*, **2019**,**143**:309-317
- [42]Xu H, Wu C K, Wei X J, et al. *J. Mater. Chem. A*, **2018**,**6**:15340-15347